UNIVERSIDAD DE INVESTIGACIÓN DE TECNOLOGÍA EXPERIMENTAL YACHAY

Escuela de Ciencias Físicas y Nanotecnología

TÍTULO: Structural and vibronic characterization of alkali-metal exfoliated GNRs dispersed in THF

Trabajo de integración curricular presentado como requisito para la obtención
del título de Ingeniera en Nanotecnología

Autor:

Andrade Guevara Denise Alexandra

Tutor:

Dr. rer. nat. Chacón Torres Julio César

Urcuquí, Septiembre 2019

SECRETARÍA GENERAL
(Vicerrectorado Académico/Cancillería)
ESCUELA DE CIENCIAS FÍSICAS Y NANOTECNOLOGÍA
CARRERA DE NANOTECNOLOGÍA
ACTA DE DEFENSA No. UITEY-PHY-2019-00009-AD

En la ciudad de San Miguel de Urcuquí, Provincia de Imbabura, a los 21 días del mes de agosto de 2019, a las 10:00 horas, en el Aula Sala Capitular de la Universidad de Investigación de Tecnología Experimental Yachay y ante el Tribunal Calificador, integrado por los docentes:

Presidente Tribunal de Defensa	Dr. ZAMORA LEDEZMA , CAMILO Ph.D.
Miembro No Tutor	Dr. REINOSO CARLOS Ph.D.
Tutor	Dr. CHACON TORRES, JULIO CESAR Ph.D.

Se presenta el(la) señor(ita) estudiante ANDRADE GUEVARA, DENISE ALEXANDRA, con cédula de identidad No. 2000118600, de la ESCUELA DE CIENCIAS FÍSICAS Y NANOTECNOLOGÍA, de la Carrera de NANOTECNOLOGÍA, aprobada por el Consejo de Educación Superior (CES), mediante Resolución RPC-SO-13-No.156-2015, con el objeto de rendir la sustentación de su trabajo de titulación denominado: Structural and vibronic characterization of alkali-metal exfoliated GNRs dispersed in THF, previa a la obtención del título de INGENIERO/A EN NANOTECNOLOGÍA.

El citado trabajo de titulación, fue debidamente aprobado por el(los) docente(s):

Tutor	Dr. CHACON TORRES, JULIO CESAR Ph.D.

Y recibió las observaciones de los otros miembros del Tribunal Calificador, las mismas que han sido incorporadas por el(la) estudiante.

Previamente cumplidos los requisitos legales y reglamentarios, el trabajo de titulación fue sustentado por el(la) estudiante y examinado por los miembros del Tribunal Calificador. Escuchada la sustentación del trabajo de titulación, que integró la exposición de el(la) estudiante sobre el contenido de la misma y las preguntas formuladas por los miembros del Tribunal, se califica la sustentación del trabajo de titulación con las siguientes calificaciones:

Tipo	Docente	Calificación
Tutor	Dr. CHACON TORRES, JULIO CESAR Ph.D.	10,0
Presidente Tribunal De Defensa	Dr. ZAMORA LEDEZMA , CAMILO Ph.D.	9,3
Miembro Tribunal De Defensa	Dr. REINOSO CARLOS Ph.D.	9,3

Lo que da un promedio de: 9.5 (Nueve punto Cinco), sobre 10 (diez), equivalente a: APROBADO

Para constancia de lo actuado, firman los miembros del Tribunal Calificador, el/la estudiante y el/la secretario ad-hoc.

ANDRADE GUEVARA, DENISE ALEXANDRA
Estudiante

Dr. ZAMORA LEDEZMA , CAMILO Ph.D.
Presidente Tribunal de Defensa

Dr. CHACON TORRES, JULIO CESAR Ph.D.
Tutor

Dr. REINOSO CARLOS Ph.D
Miembro No Tutor

CIFUENTES TAFUR, EVELYN CAROLINA
Secretario Ad-hoc

Urcuquí, 21 de agosto de 2019

SECRETARÍA GENERAL
(Vicerrectorado Académico/Cancillería)
ESCUELA DE CIENCIAS FÍSICAS Y NANOTECNOLOGÍA
CARRERA DE NANOTECNOLOGÍA
ACTA CONSOLIDADA DE FINALIZACIÓN DE ESTUDIOS No. UITEY-PHY-2019-00009-AC

En la ciudad de San Miguel de Urcuquí, Provincia de Imbabura, a los 21 días del mes de agosto de 2019, se emite la presente acta consolidada de finalización de estudios, conforme lo establecido en el artículo 101 del Reglamento de Régimen Académico aprobado por el Consejo de Educación Superior (CES), mediante resolución RPC-SO-08-No.111-2019, de 27 de febrero de 2019.

DATOS DE IDENTIFICACIÓN DEL ESTUDIANTE

Documento de Identificación	Apellidos y Nombres	Carrera
2000118600	ANDRADE GUEVARA, DENISE ALEXANDRA	NANOTECNOLOGÍA

SUFICIENCIA DE LA LENGUA EXTRANJERA

Conforme lo establecido en el artículo 31 del Reglamento de Régimen Académico aprobado por el Consejo de Educación Superior (CES), mediante resolución RPC-SE-13-No.051-2013, de 22 de marzo de 2017: (...) las IES garantizarán el nivel de suficiencia del idioma para cumplir con el requisito de graduación de las carreras de nivel técnico superior, tecnológico superior y sus equivalentes; y, tercer nivel, de grado, deberán organizar u homologar las asignaturas correspondientes desde el inicio de la carrera. La suficiencia de la lengua extranjera deberá ser evaluada antes de que el estudiante se matricule en el último periodo académico ordinario de la respectiva carrera; tal prueba será habilitante para la continuación de sus estudios, sin perjuicio de que este requisito pueda ser cumplido con anterioridad. (...) En las carreras de tercer nivel, de grado, se entenderá por suficiencia en el manejo de una lengua extranjera al menos el nivel correspondiente a B2 del Marco Común Europeo de referencia para las Lenguas. (...)

Calificación	Nivel Alcanzado
90	B2
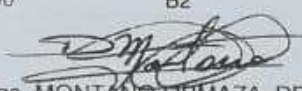
Mgs. MONTAÑO URMAZA, DENNYS EDUARDO
Director del Departamento de Inglés

PRÁCTICAS PRE-PROFESIONALES O PASANTÍAS

Conforme lo establecido en los artículos 82, 89, 94 del Reglamento de Régimen Académico aprobado por el Consejo de Educación Superior (CES), mediante resolución RPC-SE-13-No.051-2013, de 22 de marzo de 2017.

Vinculación

Empresa	Nombre Proyecto	Horas	Fecha Inicio	Fecha Fin
UNIDAD EDUCATIVA VICTOR MANUEL GUZMAN	INSPIRATHON	160	08/10/2018	08/12/2018
	Total Horas Cumplidas:	160		

Prácticas

Empresa	Horas	Fecha Inicio	Fecha Fin
FRIEDRICH ALEXANDER UNIVERSITAT ERLANGEN NUREMBERG - ANDRADE	304	04/06/2018	27/07/2018
Total Horas Cumplidas:	304		
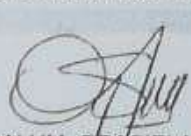
Dra. SALUM, GRACIELA MARISA, Ph.D.
Presidenta de la Comisión de Prácticas Pre-Profesionales y Vinculación con la Sociedad

REGISTRO DE CALIFICACIONES

Conforme lo establecido en el artículo 24 del Reglamento de Titulación de Grado de la Universidad de Investigación de Tecnología Experimental Yachay, en el que establece: La calificación final de grado del estudiante se obtendrá calculando de la siguiente manera: 1. El 70% corresponderá al promedio ponderado de calificaciones obtenidas por el estudiante a lo largo de toda su carrera y que se calculará en relación con el número de horas totales asignadas a cada asignatura en la correspondiente malla curricular distribuido así: a) El 20% para las asignaturas del "Tronco Común"; y, b) El 50% para las asignaturas propias de cada Carrera incluyendo los itinerarios. 2. El 30% restante corresponderá a la calificación de la defensa del trabajo de titulación o del examen teórico – práctico.

Fecha de Inicio: 28/10/2014   Fecha de Finalización: 21/08/2019

	Promedio	Horas	Créditos	Porcentaje	Calificación
Tronco Común	7,4			20 %	1,5
Carrera	8	8368	215	50 %	4
Defensa	9,6			30 %	2,9
	Calificación Final de Grado:			100 %	8,3

Mgs. CASANOVA YANDUN, EDISON GUILLERMO
Director de Registros Académicos

TITULACIÓN

Una vez se ha verificado el cumplimiento de los requisitos establecidos en el artículo 31 del Reglamento de Titulación de Grado de la Universidad de Investigación de Tecnología Experimental Yachay, aprobado mediante Resolución No.RCG-SE-10 No.036-2018 de 28 de septiembre de 2018, se confiere el título de INGENIERO/A EN NANOTECNOLOGÍA, a el(la) señor(ita) ANDRADE GUEVARA, DENISE ALEXANDRA.

Desde la fecha de suscripción de la presente acta, conforme lo establecido en el artículo 101 del Reglamento de Régimen Académico aprobado por el Consejo de Educación Superior (CES), mediante resolución RPC-SO-08-No.111-2019, de 27 de febrero de 2019; la Universidad de Investigación de Tecnología Experimental Yachay, tiene un plazo de cuarenta y cinco (45) días para registrar el título en el Sistema Nacional de Información de la Educación Superior (SNIESE), previa entrega al graduado.

Para constancia de lo actuado, firman el Secretario General, el Decano de la Escuela y el/la Estudiante.

Dr. BRITO GONZALVEZ, JOAQUIN LUIS, Ph.D.
Secretario General

Dr. MEDINA DAGGER, ERNESTO ANTONIO, Ph.D.
Decano

ANDRADE GUEVARA, DENISE ALEXANDRA
Estudiante

Autoría

Yo, DENISE ALEXANDRA ANDRADE GUEVARA, con cédula de identidad 200018600, declaro que las ideas, juicios, valoraciones, interpretaciones, consultas bibliográficas, definiciones y conceptualizaciones expuestas en el presente trabajo; así como, los procedimientos y herramientas utilizadas en la investigación, son de absoluta responsabilidad de la autora del trabajo de integración curricular. Así mismo, me acojo a los reglamentos internos de la Universidad de Investigación de Tecnología Experimental Yachay.

Urcuquí, septiembre de 2019.

Denise Alexandra Andrade Guevara
CI: 2000118600

Autorización de Publicación

Yo, DENISE ALEXANDRA ANDRADE GUEVARA, con cédula de identidad 2000118600, cedo a la Universidad de Tecnología Experimental Yachay, los derechos de publicación de la presente obra, sin que deba haber un reconocimiento económico por este concepto. Declaro además que el texto del presente trabajo de titulación no podrá ser cedido a ninguna empresa editorial para su publicación u otros fines, sin contar previamente con la autorización escrita de la Universidad.

Asimismo, autorizo a la Universidad que realice la digitalización y publicación de este trabajo de integración curricular en el repositorio virtual, de conformidad a lo dispuesto en el Art. 144 de la Ley Orgánica de Educación Superior.

Urcuquí, septiembre de 2019.

Denise Alexandra Andrade Guevara
CI: 2000118600

Resumen

Las nanofibras de grafeno o GNR (de sus siglas en inglés Graphene Nanoribbons) son tiras estrechas de grafeno que exhiben interesantes propiedades electrónicas y magnéticas debido en sus efectos de confinamiento cuántico.[1] Las cintas de grafeno pueden producirse mediante un método de deposición química de vapor(CVD), método que obstaculiza la posibilidad de obtener GNR individuales que puedan integrarse directamente a dispositivos electrónicos nanoestructurados.[2] Existen enfoques ascendentes para la síntesis de nanofibras de grafeno que han sobresalido como una alternativa a la individualización e integración de GNRs en dispositivos electrónicos cuánticos.[3,4] Los métodos existentes para obtener GNRs de una capa o para su individualización desde paquetes enredados de este material pueden ser costosos y/o no recomendables para su producción a gran escala.[4] En este trabajo se ha buscado optimizar el proceso de dispersión de GNRs obtenidos por CVD en Tetrahidrofurano(THF) a través de un mecanismo de transferencia de carga utilizando sodio y potasio como especies donantes de electrones para individualizar y obtener nanofibras de grafeno individualizadas desde paquetes enredados de este material.

Palabras clave: Graphene nanoribbons, intercalación, dispersión, THF, metales alcalinos.

Abstract

Graphene Nanoribbons (GNRs) are narrow strips of graphene that exhibit interesting electronic and magnetic properties based on its quantum confinement effects.[1] GNRs can be produced by a chemical vapor deposition method (CVD), which for instance hampers the possibility to get individual GNRs that can be directly integrated to nanostructured electronic devices.[2] There exist bottom-up approaches along the synthesis of GNRs that has excel as an alternative to single individualization and integration of GNRs into quantum electronic devices.[3,4] These existing methods to obtain single monolayer GNRs or to individualize bundles of CVD grown GNRs, can be expensive and/or not suitable for a scalable production[4]. In this work we have optimized a dispersion process for CVD grown GNRs in tetrahydrofuran (THF) *via* a charge transfer mechanism method using sodium and potassium as electron donor species to individualize and get single dispersed graphene nanoribbons from bundles.

Keywords: Graphene nanoribbons, intercalation, dispersion, THF, exfoliation.

Acknowledgements

I am grateful to all of those with whom I have had the pleasure to work during this project. I am grateful to my university, and all the wonderful professors I had found on my way. I would like to recognize the great importance for this achievement of Claudia Kröckel and the Joint Institute of Advanced Materials and Processes (Zentralinstitut für neue Materialien und Prozesstechnik, ZMP) of the University Erlangen-Nuremberg who provided me of tools and primordial knowledge to make this project possible. I would especially like to thank Dr. Julio C. Chacón-Torres, a role model of dedication, and a great guide in my career during these last years. He has taught me much more than I can thank. Finally, I would like to thank my beloved family, who have supported and guided me on this journey. They provided me with safety and love during these years of my career. I would not have achieved it without them.

Contents

List of Figures

List of Tables

List of Papers

[1] Andrade Guevara, D.; Kröckel, C.; Hauke, F; Hirsch, A. Chacón-Torres, J.C. Structural and vibronic characterization of alkali-metal exfoliated GNRs dispersed in THF. In preparation.

Chapter 1

Introduction

Carbon nanomaterials have aroused interest in the scientific community in last decades.[5] The versatility and variety of configurations and properties obtained in these carbon materials due to the hybridization possibilities gave them surprising electronic, magnetic and optical properties.[1] High electric and heat conductivity place these materials as very promising for current and future of electronics. The crystalline hybridizations of carbon form diamond, fullerenes, graphite and a one layer thick sheet of graphite being called graphene. Graphene is a sp^2 hybridized carbon material which posses carbon atoms arranged in a hexagonal pattern. A variation of this material are Graphene Nanoribbons (GNRs), whose consist in narrow strips of graphene that exhibit interesting electronic and magnetic properties based on their quantum confinement effects.[3] This material is very especial as its edges allow the possibility of functionalization and particular electronic properties which open a wide range of possibilities for applications.[6] Also, the control on the edge shape defines the character of the material, whether metallic or semiconductor.[5] The production of individual GNRs is already possible through bottom up approaches which are often very expensive and/or not suitable for scalable production. GNRs produced by Chemical Vapor Deposition (CVD) result in entangled GNRs and lot of other carbon byproducts. Those obstacles make almost impossible the use of this material for industrial purposes.[3] for the individualization of a material of the same structure, single layer graphene from graphite, several methods has been reported. Graphite intercalation compounds exfoliation has shown to be a very effective method to obtain graphene. Introducing an anion into the interlayer spaces provoke the expansion of the spacings between the graphite layers. Cation, also introduced in the structure make the graphite

1

layers weakly bonded, then can be separated by ultrasonication. Liquid-Phase exfoliation process are also been used to obtain individual graphene layers. Sonication is used to induce physical or chemical change in the system, in this specific case by generating cavitation bubbles. It results in shock waves and high-speed microjets which produces shear forces on graphite.[7] It was reported that Van der Walls forces among graphite layers can be also overcome by minimizing the interfacial tension between the material and a solvent. This is achieved by some organic solvents as Tetrahydrofuran (THF).[7,8] Those methods have served as guide to develop a new synthesis process based on the knowledge of Intercalation and Exfoliation interaction with the material. The intercalation process on GNRs consist in the inclusion of extra charges between the layers of the carbon allotrope creating a different regime of electronic forces which not only provide from extra properties to the material, but also gave them the possibility to counterbalance the Van der Waals forces in their structure.[8] The chemical exfoliation of the intercalated material can be done using aprotic polar solvents, in this case THF, allowing the obtaining of individual or at least thinner layers of the primary material.[9] In the case of GNRs, the intercalation/exfoliation process allow the fiber individualization.

Graphene nanoribbons characterization can be performed using transmission electron microscopes (TEM) and Raman spectroscopy. It is advantageous for distinguishing zigzag from armchair edges, also for stacking determination through its diffraction pattern.[10] Scanning tunneling microscopy (STM) and spectroscopy (STS) are also powerful tools to identify defects, layers number, conduction character, and edge termination in nanoribbons.[11] XPS is also used to obtain information about addition functional groups and sp^2/sp^3 ratio.[6] GNRs can also be characterized by using SEM and AFM. Those tools permit to vizualize the structure and morphology of the bulk or individual material. Invidualized samples are aslo easily seen even in an optical microscope of good resolution.

The objective of this work is to find and optimize a dispersion process for CVD grown GNRs in tetrahydrofuran (THF) *via* a charge transfer mechanism method using sodium and potassium as electron donor species to individualize and get single dispersed graphene nanoribbons from bundles as it will be shown along this project report. Graphene nanoribbons produced by CVD were intercalated with alkali metals (Na and K) in different proportions and exfoliated by dispersing the GNRIC in THF and sonicating the solution. This procedure is effective producing individualized GNRs from both intercalation compound. The obtained GNRs excel by its ribbon-like

morphology, the amount of individualized structures produced and its great length.

Chapter 2

Theoretical Principles

2.1 Carbon Materials
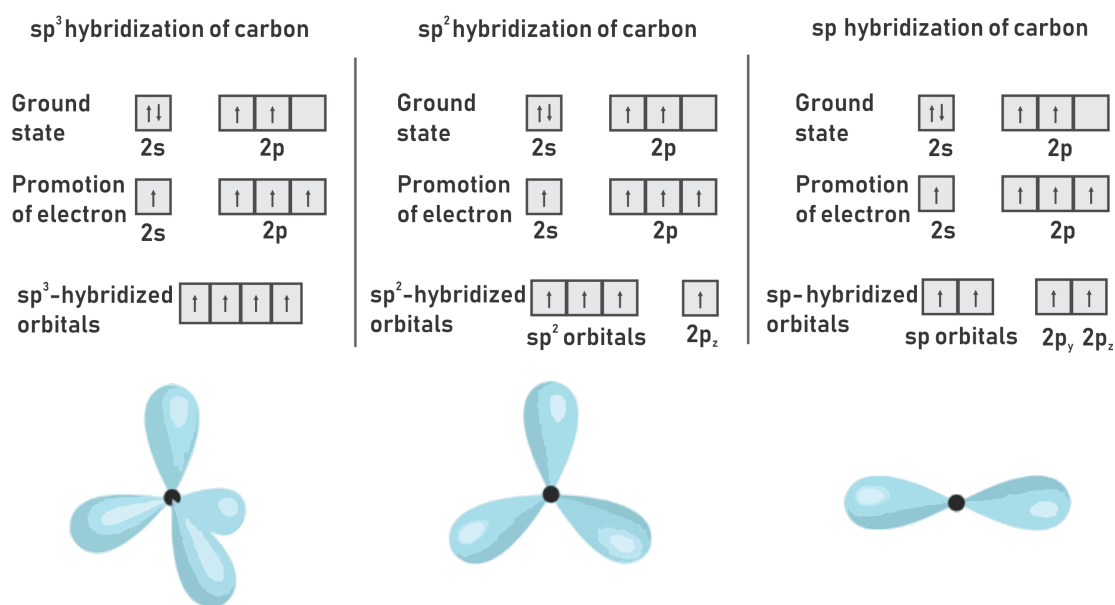
Figure 2.1: Hybridization of orbitals of a carbon atom. Adapted from reference [6]

Carbon is the fourth most abundant element in the universe and the base of life on earth.[5]

Located in the group IV of the periodic table, it own 6 protons and electrons which make its last shell unfiled by 4 electrons, providing this element with a valence 4. Its electronic configuration is $1s^2 \, 2s^2 \, 2p_x \, 2p_y$ in the ground state.[12] Carbon can form linear, trigonal planar and tetrahedral structures as the most common ones.[5] Carbon can be found in amorphous and crystalline forms, being graphite the most thermodynamically stable form. The role of the most external electrons placed in the 2p orbital is fundamental to the formation of bonds. From here arises the concept of hybridization which explains the superposition of the 2s and 2p orbitals in an excited state. In sp^3 hybridization, one electron moves to the empty p orbital, completing a very stable form with each p orbital filled and combined with the s orbital. In sp^2, s, p_x and p_y orbitals combine and left one electron in the p_z orbital which transform into a perpendicular localized orbital with respect to the other ones. Finally, in sp hybridization, two p orbitals combine to form a triple bond. Carbon can form sp, sp^2 and sp^3 hybridized orbitals as shown in Figure 2.1. This configuration allows the existence of diamond, graphite, fullerenes, carbon chains besides amorphous forms and other configurations based on graphite like graphene, carbon nanotubes and graphene nanoribbons.[5]

Diamond is an sp^3 allotrope of carbon, extremely hard, due to the 3-dimensional covalent network
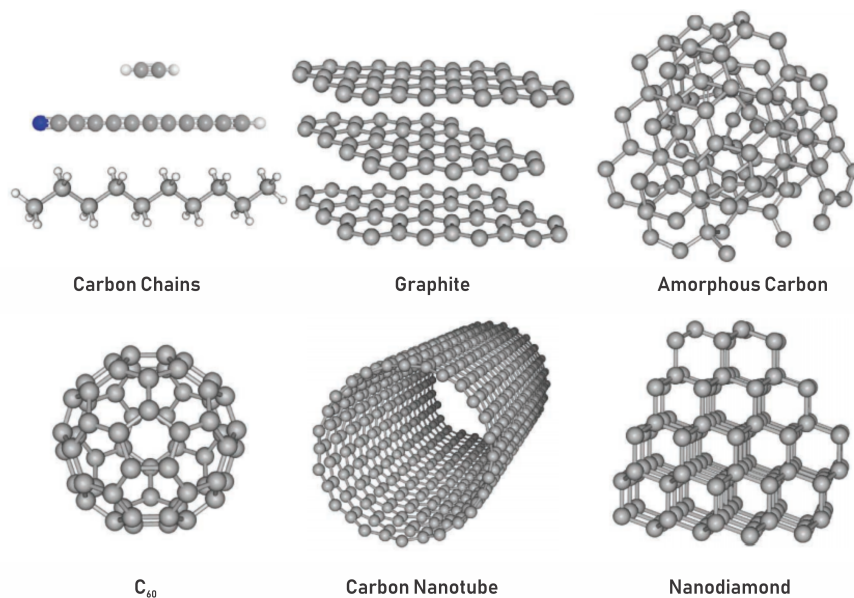
Figure 2.2: Schematic illustration of individual carbon allotropes. Adapted from reference [19]

in its crystalline structure. It also does not have free electrons, which make it not conductive and transparent as there are no free electrons which could absorb radiation. Graphite [Fig 2.2] which possesses an sp^2 structure, free π-electrons allow conduction and absorption of all radiation in the optical region.[13] sp^2 hybridization also allow the existence of other kind of structures as carbon nanotubes [Fig. 2.2] which posses excellent mechanical stiffness and tensile strength due to its bonding and structure. They also posses a high electrical conductivity and thermal conductivity as graphite and other materials with this hybridization. Carbon can also exist as carbyne, an sp hybridized chain of carbons [Fig. 2.2] which are predicted to have an ultra high thermal conductivity[14] and to be the strongest nanowire existent.[15] Even mixtures of sp^2 and sp^3 hybridizated carbon atoms which posses no crystalline structure are useful in science. Amorphous carbon [Fig 2.2] when deposited in films (Diamon-like carbon), can present microhardness and elastic modulus which make it usefull to coat other materials.[16] It can also show mechanical hardness, and wider bandgap than sp^2 materials.[17] Amorphous carbon can lead to other structures of combined hybridezed carbon as fullerens [Fig. 2.2] by photochemical processing of its hydrogenated.[18]

In general, carbon allotropes possess amazing electronic, magnetic and optical properties. Conduction properties of electricity and heat placing these materials as very promising for future electronics. Then, it is evident the importance of the hybridization, bonding and the configuration of the multifaceted carbon.[5]

2.2   Graphene
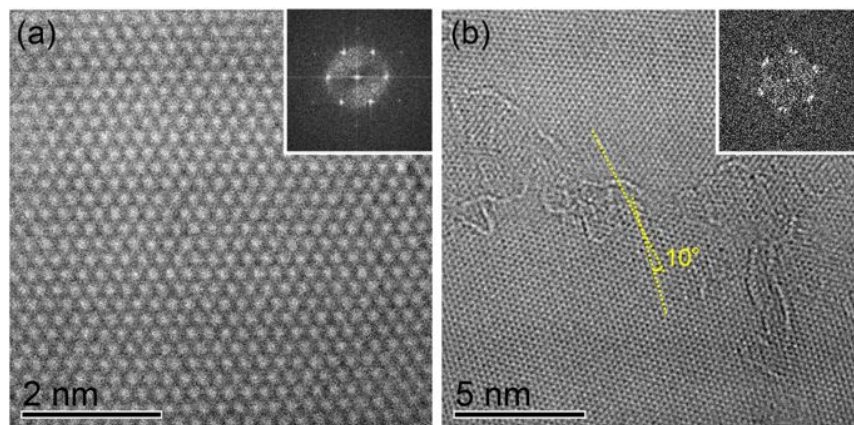
Figure 2.3: a) HR-TEM image of graphene film and (b) its grain boundary with its corresponding diffraction patterns. The misoriented angle shown between graphene domains in the (b) diffraction pattern is within 10 degrees.[19] Adapted from reference [5]

Graphene is a 2D single layer of sp^2 hybridized carbon nanomaterial with hexagonal packed configuration [Fig. 2.3]. The geometry of this material is trigonal planar with a 120° bond angle between the hybrid orbitals. The investigation conducted by Geim and Novoselov about this material has proven it is the building block for all graphitic carbon materials such as graphite, diamond, nanoribbons, CNTs, and fullerenes.[5] Extraordinary properties, such as a high charge carrier mobility, high thermal conductivity, and excellent mechanical flexibility make them attractive for a range of applications.[5] Remarkable aspects about this carbon materials is the charge carrier density and carrier mobility, which in graphene are very high[20] due to the a free electron in the z direction called (π)-electron. Their conduction and valence band collide at the K points of the Brillouin zone, forming the so called Dirac cone.[3,5] This zero band gap point make it semimetallic. However the band structure of graphene can be modulated by modifying the width of the graphene layer into a ribbon like shape.[6]

2.3   Graphene Nanoribbons Structure and Properties
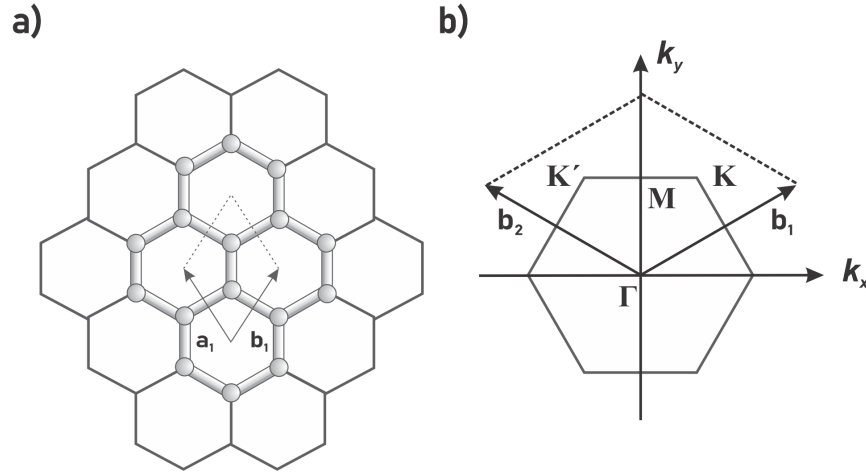
Figure 2.4: (a) The lattice structure and the unit cell vectors of graphene and its (b) corresponding Brillouin zone with the special high symmetry points Γ, M, K, and K'.Adapted from reference [6].

Graphene nanoribbons are narrow strips of graphene that exhibit interesting electronic and magnetic properties based on their quantum confinement effects.[3] Graphene's hexagonal lattice and its reciprocal lattice are shown in Figure 2.4. The lattice vectors for this material are $a_1 = a(\frac{\sqrt{3}}{2}, \frac{3}{2})$ $a_2 = a(-\frac{\sqrt{3}}{2}, \frac{3}{2})$ that correspond to the distance between the lattice points a= 1.42. In its reciprocal lattice, the corresponding lattice vectors are $b_1 = \frac{2\pi}{3a}(\sqrt{3}, 1)$ and $b_2 = \frac{2\pi}{3a}(\frac{1}{\sqrt{3}}, 1)$. The distance between the points in the reciprocal space are inversely proportional to the lattice distance in the real space as expressed by the vectors. The high symmetry points in the reciprocal lattice are of a high importance as the energy dispersion becomes linear in those points giving rise to the outstanding electronic properties of graphene.[21]
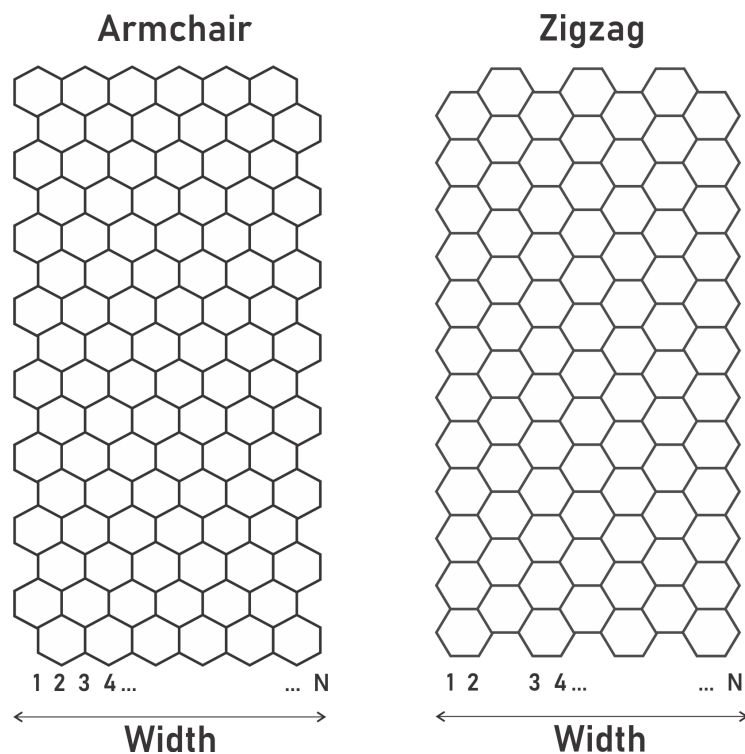
Figure 2.5: Graphene Nanoribbons (armchair and zigzag) structure. Adapted from reference [21].

GNRs, as graphene, possess a honeycomb structure which results in two possible edge structures: armchair and zigzag[5,22] [Fig 2.5]. The shape of this edges can determine the character of the GNR, being semiconductors when armchair edges are present and metallic in the other cases.[5] Other chirality are allowed to exist, however they are not so stable as the aforementioned.[23] Reducing or increasing one dimensionality on graphene rise as a new possibility to control the character of the material. The energy gaps of GNRs are inversely proportional to the ribbon width.[24] GNRs longer than 5 microns showed a metallic character.[25] Then, controlling the shape of this material allow us to engineer their band structure. Thus, potential applications in electronics become evident when you bring out the behavior of electrons acting as photons.[5] These electrons show high carrier mobility, which means that they travel with no resistance, even at room temperature and can move without scattering through ten hundreds of micrometers[5], having less energy dissipation.

Zigzag graphene nanoribbons posses localized edge states close to the Fermi level which called the atention as magnetic material, different to armchair GNRs where their edge state is absent.[26] The continued down-scaling of the features on semiconductor chips expected arises the need of low dimensional materials like carbon nanotubes and GNRs to replace the widely used Cu, which seems obsolete in this context.[5] GNRs show higher conductivity, resistance to electromigration due to the strong inherent carbon-carbon bonds, an extraordinary mechanical strength, a very large current conduction capacity of 109 A/cm^2, higher than Cu conduction capacity in three orders of magnitude and a in-plane thermal conductivity of approximately 5000 W/mK, also larger than Cu.[5] Zero-conductance Fano resonances shown by GNRs made them useful to build nanojuction structures for semiconductor devices. This ability is used for current-controlling switching in diverse devices.[26] All those properties explain the great interest of working with this material nowadays.

2.4 Fabrication Methods for GNRs

2.5 Chemical Exfoliation Method for Graphene Fabrication

Chemical exfoliation to obtain graphene was already reported as a successful method to obtain high-quality material at low cost.[7] Liquid phase exfoliation consists in the dispersion via sonication of a previously dispersed solution of graphite with an specific solvent. Sonication is used to induce physical or chemical change in the system, in this specific case by generating cavitation bubbles. The sonication process can be tip or bath sonication. The growth and collapse of microbubbles induced during the process of sonication is called cavitation-induced pressure pulsation. It results in shock waves and high-speed microjets which produces shear forces on graphite[7], capable to "peel" the layers of this material to form graphene. Exfoliation can be also be preceded by intercalation of graphite. Salt-intercalation exfoliation of graphite consist in the introducing an anion into the interlayer spaces and expand the spacings between the graphite layers[27]. Cations insert themselves within the graphite layer and form expanded graphite. Then, weakly bonded graphite layers are then separated by ultrasonication.[27] Inclusion of anions to change charges distribution is in general favorable to perform exfoliation. The intercalation process can be done also by other electron donor species or molecules.[27] Another method recently

presented allow the production of graphene nanosheet of fewer than three layers thickness by combining micro-jet cavitation and supercritical CO_2.[7] The mechanism of exfoliation graphene without supercritical CO_2 can lead to defects on the structure done by the micro-jets which would perforate the structure. In the other case, The collision of molecules between the layers caused by the turbulence of a fluid in a nozzle provoke the relaxation of Van de Walls forces of graphite, allowing the layers to separate.[7]

Van der Walls forces can be overcome by minimizing the interfacial tension between the material and a solvent. This is achieved by some organic solvents as N, N-dimethylacetamide, 4 N,N-dimethylformamide (DMF), Dimethylsulfoxide (DMSO), Ortho-dichlorobenzene and Tetrahydrofuran (THF) among others.[7,8] But a serious challenge to overcome is the low concentration of graphene dispersions obtained, generally, less than 0.01 mg /mL.[7] Fortunately, the efficiency of these methods can be improved by adding auxiliary agents as the aforementioned sonication and intercalation process. This enables the possibility of performing a more successful method based on the processes already explained.

2.5.1 Bottom-up approach
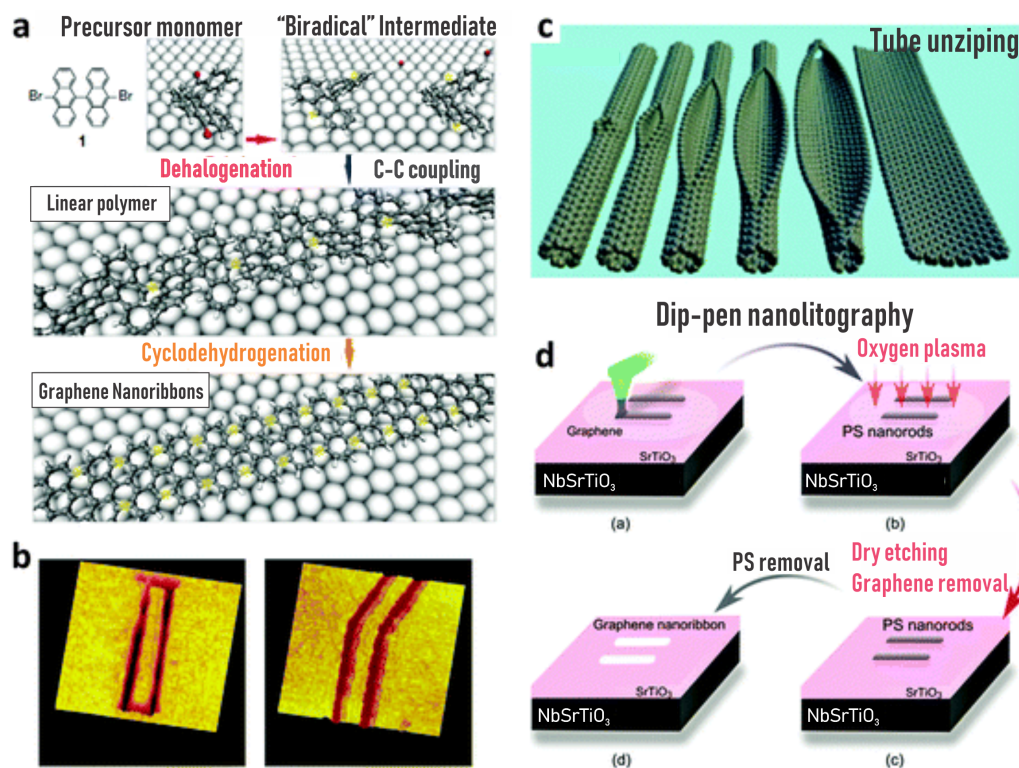
Figure 2.6: Methods to obtain Graphene nanoribbons. (a) Chemical synthesis from selected monomers. (b) STM lithography. (c) Unzipping of CNTs. (schematic image). (d) Dip-pen nanolithography. Adapted from reference [27]

There exist bottom-up approaches along the synthesis of GNRs that have excel as an alternative to single individualization.[3,4] Among these methods are lithography and polymerization which allow the atomically precise production of GNRs with a width in the range of atoms and sharp edges. Those methods consist on patterning with nanometer-precision and determining crystal orientations over a substrate. Lithography uses an electron beam to draw custom shapes over an electron-sensitive film to deposit carbon material [Fig 2.6 (b)]. This customization of the

edges gave it advantages over other methods, but the product is mostly too short and the process is costly.[28,29] The polymerization method uses a precursor monomer over a gold substrate and forms GNRs through dehalogenation and cyclodehalogenation pocesses[Fig. 2.6 (a)].[10?] These existing methods to obtain single monolayer GNRs or to individualize bundles of CVD grown GNRs can be expensive and not suitable for a mass scale production,[3] becoming necessary the develop of new methods to improve GNRs production.

2.5.2   Top-bottom approach

GNRs can be produced by top-bottom methods as chemical vapor deposition (CVD).[6] The method consists of the decomposition of a gas containing $CO/H_2/Fe(CO)_5$ at $400 - 700°C$. A solution of 2.80 g of ferrocene and 0.26 mL of thiophene in 280 mL of ethanol can be used to form the pyrolitic solution for the synthesis. The aerosol generated ultrasonically is carried by an argon flow into a quartz tube located inside of a two-furnance system heated to 1223 K. The ultrasonic sprayer is then turned down after 30 minutes, the argon flow decreased and the furnance is cooled down. Finally, the material is scraped of the quartz tube.[6] This CVD process is well established and high quality GNRs can be produced.[6] Our pristine material was synthezized this way by Dr. Maria Luisa Garcá Betancourt from the CIQ-VAEM Mexico. Unzipping of multi-walled carbon nanotubes (MWCNTs) along their longitudinal direction is an alternate option to synthesize graphene nanoribbons[Fig. 2.6 (c)]. MWCNTs are unzipped by a chemical treatment with H_2SO_4 and $KMnO_4$. The produced ribbons contain oxygen chemical groups damping the electrical conductivity, generating the need for a reduction or annealing post process in hydrogen to remove those groups. Top-down production approach allows the massive generation of GNRs, however, these are usually intertwined between them which for instance hampers their possibility to be used individually to be directly integrated to nanostructured electronic devices.[2]

2.6   Graphene Nanoribbons Exfoliation in THF
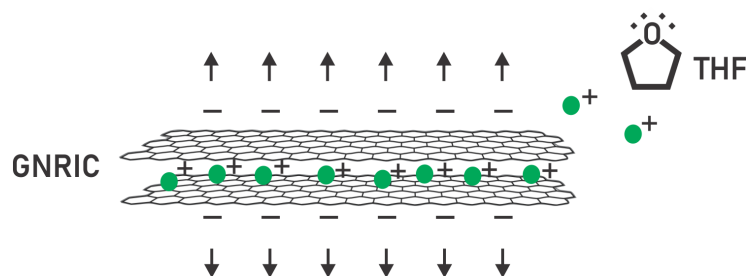
Figure 2.7: THF and GNRIC scheme. The charges involved in the exfoliation of the compound

Tetrahydrofuran (THF) is a dipolar aprotic organic solvent with chemical formula C_4H_8O. It is obtained by the hydrogenation of furan or dehydratation of intramolecular 1,4-butanodiol. THF is a very reactive solvent when exposed to light as it forms radicals. Its density and molar mass is about 889 kg/m^3 and 72.11 g/mol respectively. THF is a Lewis base, capable to accept positive charges as the oxygen molecule in its structure posses unshared electrons[30] [Fig.2.7]. The alkali metal that act as electron donor get positively charged when intercalated in the graphene nanoribbon structure. The positive charges leave the estructure to bond with the THF unshared electron pairs provoking the separation of the layers of GNRs layers and dispersion of the bundles.

2.7   Characterization Methods

2.7.1   Atomic Force Microscopy
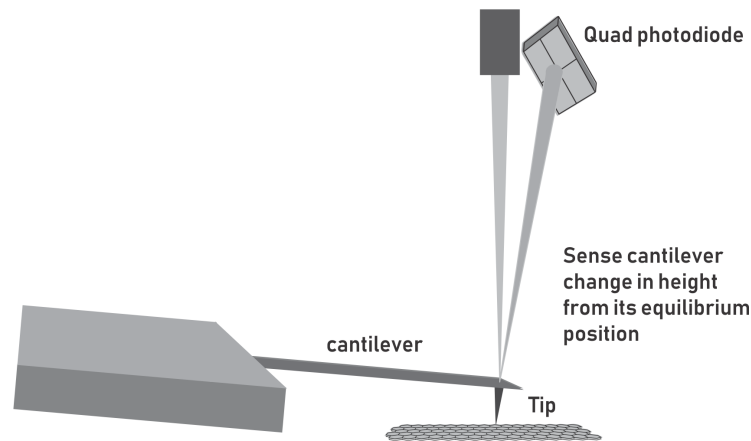
Figure 2.8: AFM working principle scheme. Adapted from reference [31]

Atomic force microscopy (AFM) is a very high-resolution microscopy method used to measure forces in the order of 10^{-18}N.[31] It consists of a cantilever with a sharp tip which is used to map the topography of the specimen [Fig 2.8]. When it approaches the sample surface, the forces between the tip and the sample provoke the deflection of the cantilever which is transformed into an electrical signal when comparing this displacement to the equilibrium position.[32] Those forces could be Van der Waals, capillary, chemical electrostatic or magnetic, among others. A tunneling tip is attached to the cantilever. This tip is fixed to a piezoelectric element which drives the cantilever beam at its resonant frequency.[31] According to the sample needs it is possible to use different imaging modes possible due to the cantilever oscillation at given frequencies.[31] The contact mode is the simplest operational method used. The tip tracks the surface and the deflection of the cantilever is detected directly. The cantilever deflection is kept constant by retracting or elongating the z-piezo. The feedback algorithm compares the reference value with the actual signal to determine the desired movement through the z-piezo voltage lecture. This last step is then transformed in to the topographic data of the image.[33]

When the sample requires a stealth approach because there exists a risk of staking, it is most

likely to use a Tapping mode. In this dynamic mode, the cantilever oscillates near to its resonance frequency using a piezoelectric element, a laser modulated heating or a magnetic field[32]. The cantilever oscillation amplitude changes with sample surface topography. The cantilever displaces to the distance between oscillating tip and sample to keep the tip amplitude constant.[32] The resulting AFM image is produced by imaging the force of the intermittent contacts but also taking into account the phase shifts done by the *z*-piezo.[32]

A special dynamic mode used for delicate tip-sample interaction requirements is a non-contact AFM. The cantilever oscillates at its resonant frequency or above, at a few nanometers oscillation amplitudes. Only attractive forces are sensed as it does not approach enough to impact the surface. The attractive interaction affects the resonant behavior and provokes a decrease in the phase oscillation enabling the topography traction.[32]

2.7.2   Scanning Electron Microscopy
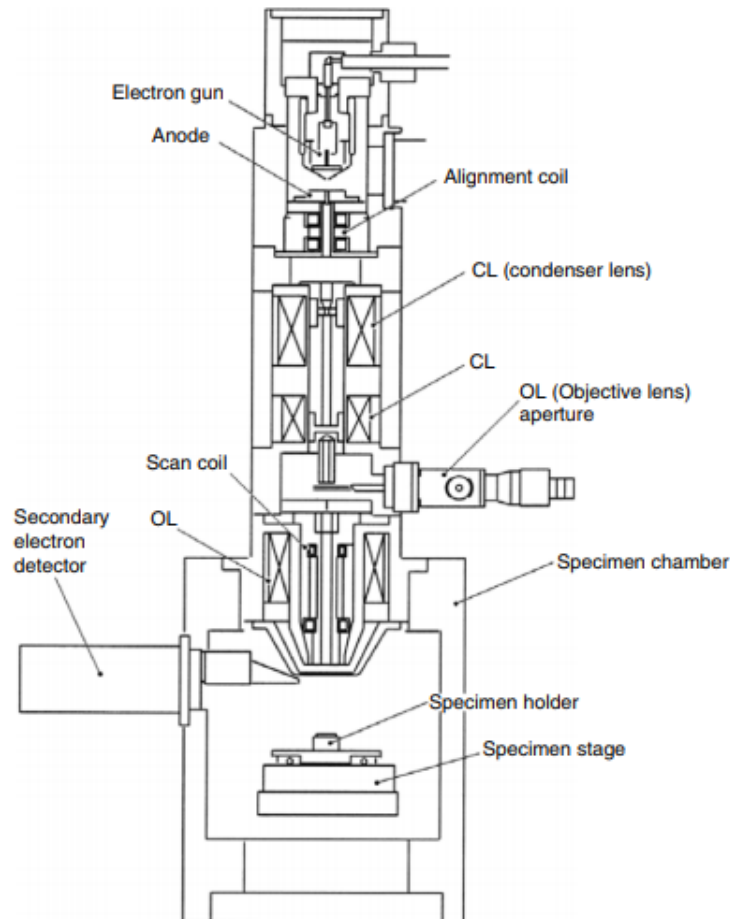
Figure 2.9: Set-up of a Scanning electron spectrometer. Adapted from reference [33]

Scanning electron microscopy (SEM) is a versatile technique useful for analysis of microstructure morphology and chemical composition.[34] This artifact of column structure poses an electron gun at the top which produces electrons and accelerates them. This electron source could be an electron gun, popularly formed by tungsten or lanthanum hexaboride or a field emission system. The electron gun chosen varies in the current produced, energy dispersion, lifetime and price.[34] The beam produced is too large to form the expected resolution, then is reduced through

electromagnetic lenses to be focused over the specimen. The microscope poses condenser lenses to converge and collimate the beam into a parallel stream. The lens is formed by two rotationally symmetric iron pole pieces with a copper winding which provide magnetic field. Objective lenses are part of the equipment likewise to focus the electron beam into a probe point [Fig. 2.9]. A correct choice of lens demagnification and aperture size results in a reduction of the beam diameter and resolution enhancement.[34] Diverse beam parameters influence the quality of the obtained image, those are electron beam energy, current, aperture size, working distance, and lens aberration. The sample is placed in a high vacuum environment. The signal detection at real-time allows the observation and recording of the specimen surface. The signal to be detected is generated by the interaction of the electron beam with the specimen, which provokes an excitation of the specimen surface. This interaction is produced also under the surface, the volume affected depends on the composition of the sample, the energy and the angle of the beam. There exist two kinds of scattering process which can be used to form an image, elastic and inelastic. Elastic interaction produces backscattered electrons, which give you information of the sample composition through the image contrast while inelastic interaction produces secondary electrons, which are of low energy and give you information of the surface topography of the sample. The beam interaction also produces x-rays, which produce signal capable of decode the sample composition proportion of the whole sample or a single spot through an Energy dispersive detector (EDS).[34]

2.7.3   Raman Spectroscopy
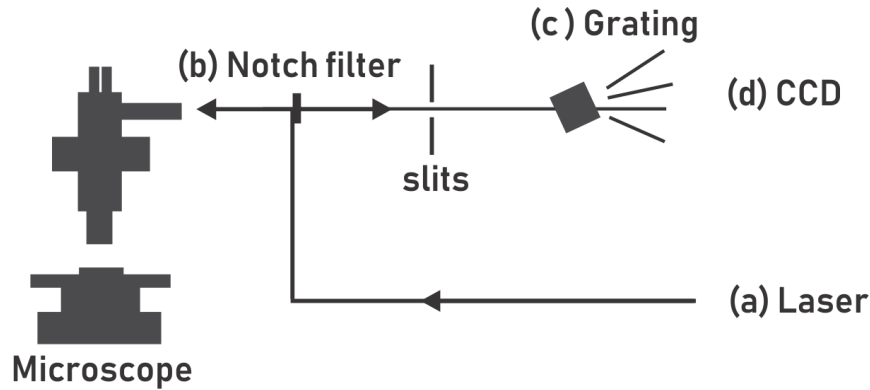
Figure 2.10: Set-up of a Raman spectrometer. Adapted from reference [37]

Raman spectroscopy is a widely used method for investigation and industrial applications to determine the exiting vibrations in the crystal lattice of a nanostructure. Raman spectrometer uses a laser at an specific wavelength which ranges from ultraviolet (UV) to the near-Infrared. This selected beam [Fig. 2.10 (a)] will be focused on a filter which will reflect the light at a right angle. The light scattered passes a band-stop filter [Fig. 2.10 (b)] which attenuates the beam. Raman scattered light is redirected through mirrors to a monochromator [Fig. 2.10 (c)] which diffracts it into a narrow band of wavelengths to be measured by the detector [Fig. 2.8 (d)].[35] The final result is a Raman spectrum.

The irradiation of photons of known energy provokes an interaction with matter that may result in the absorption, scattering or no interaction.[35] Different energies are related with different optical transitions, giving rise to the different spectroscopic branches. From 10 meV to higher energies than 20 eV the photons are absorbed to create extending phonon modes or to excite electron in the lattice to produce infrared absorption or excited photoelectrons in extreme cases.[23]

The Raman scattering involves a light scattering process produced by optical phonons where a polarizable sample "absorbs" a part of the phonon energy inducing a transition from the ground electronic state to an excited state which then will decrease to a lower energy by the emission of a photon.[35]
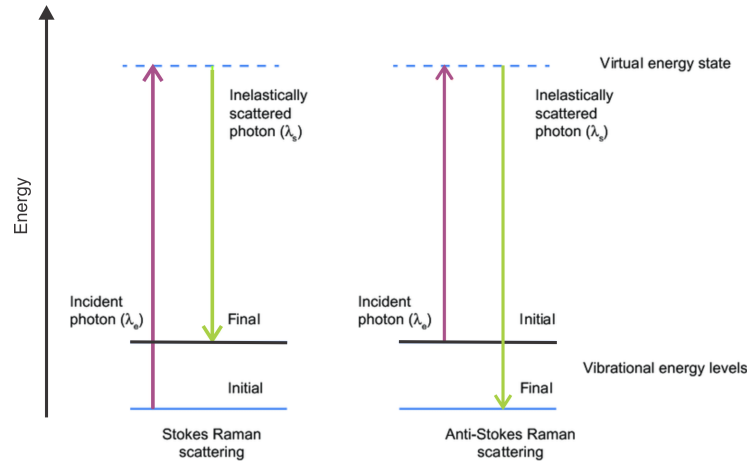
Figure 2.11: Stokes and Anti-Stokes process. Adapted from reference [35]

The phonon energy produces the movement of atoms in the sample. The transmission of energy and momentum induce the excitation of the medium creating (Stokes process) or absorbing (anti-Stokes process)[36] [Fig 2.11] a vibrational quantization of energy when the light scatters inelastically or elastically (Rayleigh scattering). The Plot of the scattered intensity of the present phonon modes with respect to the energy in cm⁻1 produce a Raman spectrum.

Raman Spectroscopy in Carbon nanomaterials
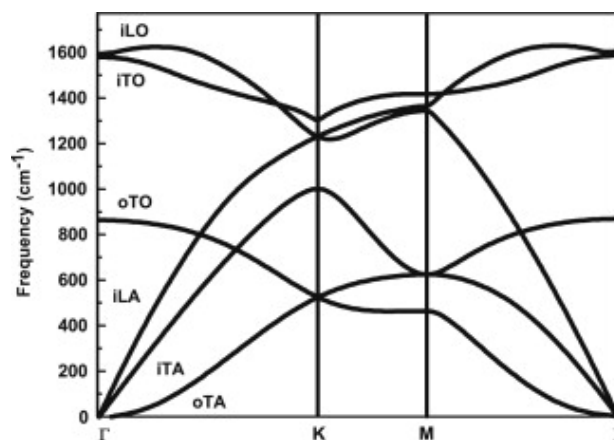
Figure 2.12: Phonons dispersion relations for graphene. Adapted from reference[36]

In the particular case of allotropes of carbon the resulting spectrum exhibit typically three Raman modes: D-band (1350 cm^{-1}), G-band (1580 cm^{-1}) and 2D-band (2700 cm^{-1}).[6,23] Those modes are caused by the average of phonons at the high symmetry Γ or K points and its proximity. The possible phonon vibration produced by energy addition correspond to in-plane and out of plane transversal modes (iT оT) and in plane longitudinal modes (L) [Fig. 2.12] for optical and acoustic vibrations.[23,37] Following, the most important Raman modes present in carbon materials spectrum will be explained.

The G-band

The G-band is present in all sp^2 nanocarbons at around 1580 cm^{-1}. The vibration corresponds to the transverse in-plane optical phonon (iTO) and the longitudinal optical (LO) phonon, rising from the in-plane C-C streching mode. This frequency is high as correspond to the vibration of a strong covalent bond of small mass atoms.[23] The iTO and LO phonon fequencies at the center of the Brioullin zone in sp^2 carbon materials are the same. However, they are degenarate at Γ in graphite and graphene. Under strain situations, both modes combine and give raise to a new frequency with splits into two peaks as the strains increase. In Carbon nanotubes, strain is always present because of the curvature effect. Rolling up a graphene sheet would lead to an splitting of the G-line, differentiated from graphene by the phonons produced for each carbon nanotube's (CNT) chirality. The temperature, and doping on graphene can cause the red-shift, blue-shift and/or the change in the linewidth of this Raman feature. In the case of high temperatures, the spectral line decreases in frequency, being reduced for an n-type doping, p-type dopping is detected by a blue-shift of the G-line position.[23]

The D-band

The D-band appears typical in the range of 1250 cm^{-1} to 1400 cm^{-1} and show the disorder-induced in the lattice component. Those symmetry break on the graphene structure lead to the activation of phonon modes which are not Raman active creating new scattering processes. Its frequency vary as the laser energy and the intensity of the band can be related with the amount of disorder present in the lattice. The ratio between this band and the G-band allows to compare the defect ratio and therefore the crystallinity of the sample. A double resonance process derived from this frequency appear at higher wavenumbers.[23,38]

The 2D-band

It corresponds to a second order phonon process located at 2500-2800 cm^{-1}, It dependens on the laser excitation energy and is part of the higher-order Raman spectra. The excitation of an electron form the valence band to the conduction band maintain the energy transferred in graphene related systems as it does not posses an energy gap. The energy emitted as a phonon connects two conduction electronic states. This phonon scattering will be resonant. In stacked structures, the sensitivity of this mode allow the determination of layers in the material. In case of doping, the 2D line blue-shifts or red-shifts depending on the type of doping environment. The increment on the size of the line can determine the concentration of the dopants.[23]

Radial Breating Modes (RBMs)

Carbon nanotubes present phonon processes at 50-760 cm^{-}1. As suggested by its name, in the radial breathing mode (RBM) carbon atoms of a CNT vibrate with the same phase and radial direction. Because of the one-dimensional character of carbon nanotubes, the RBM spectra are extremely informative about resonance Raman phenomena. Specific RBMs are related to chiralities, radii, polarization and tube-tube interaction. The Raman spectral width is given by the lifetime of phonons.[23] The peak intensity is laser dependent, and its broadening could depend on temperature effects, tube-tube substrate interaction or defects and interstitial impurities.[23] The RBM frequency shift due to doping. Changes due to temperature or strain are normally not representative.

Chapter 3

Motivation

The great attention that GNRs had obtained by the versatility and their tunable properties already discussed in chapter two, make them a very promising material for applications as nanojunctions, electrodes, connections, among others. The width, length and edge shape of a GNR is decisive to determine its quality and electronic properties. There exist bottom-up approaches along with the synthesis of GNRs that has excel as an alternative to single individualization and integration of GNRs into quantum electronic devices.[3,4] Lithography, polymerization, and oriented growth are methods that allow the creation of atomically precise GNRs, nevertheless, the price associated to its synthesis is very high in addition to the difficulty of bulk production through those methods.[10] In the other side, top-bottom methods as CVD and unzipping allows the obtaining of a great amount of GNRs but mostly not individualized, which make them unusable.[3,10] As the existing methods to obtain individualized GNRs are expensive and not suitable for a mass scale production[3], then is necessary to design a new procedure. In this project, it is proposed to perform an intercalation/exfoliation process of graphene intercalation compounds with sodium and potassium dispersed in THF with the aim of obtaining individualized GNRs from CVD GNRs. As the existing methods do not reach to fulfill the needed characteristics on the material, this proposal is presented expecting to obtain individualized GNRs of great length and physical characteristics through a simple synthesis method. Intercalation/exfoliation process is also low-cost and allows to obtain GNRs for scalable production from bulk CVD GNRs.

Chapter 4

Methodology

4.1 Synthesis
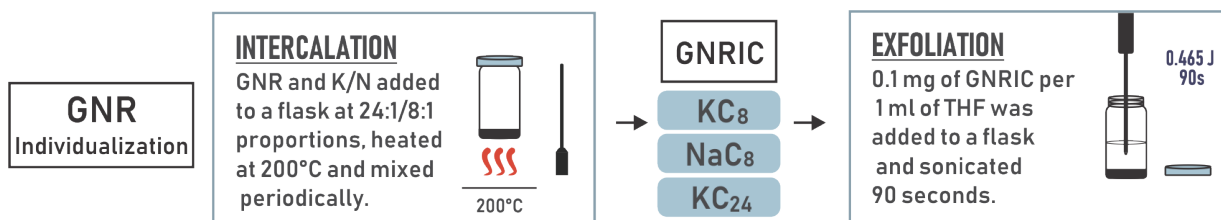
Figure 4.1: Intercalation/Exfoliation process

The complete experiment was carried out in an argon-filled glovebox (<0.1 ppm of H_2O and O_2) at room temperature. GNRs used in this experiment were obtained from Dr. Maria Luisa García Betancourt from CI1-UAEM Mexico. The graphene nanoribbons, produced by chemical vapor Deposition[6], were mixed with alkali metals (Na and K) in a glass vial in three proportions: a) 11.38 mg of GNRs per 2.73 mg of sodium (NaC_8), b) 3.2 mg of GNRs per 1.3 mg of potassium (KC_8) and c) 13.4 mg of GNRs per 1.87 mg of potassium (KC_{24}). The mixtures were placed in a heating plate where the temperature was slowly increased up to 200°C. The samples were then stirred carefully every 20 minutes during one hour. The samples were kept at 200°C in the hot plate during 48h to get an homogeneous intercalation compound[9] [Fig. 4.1].
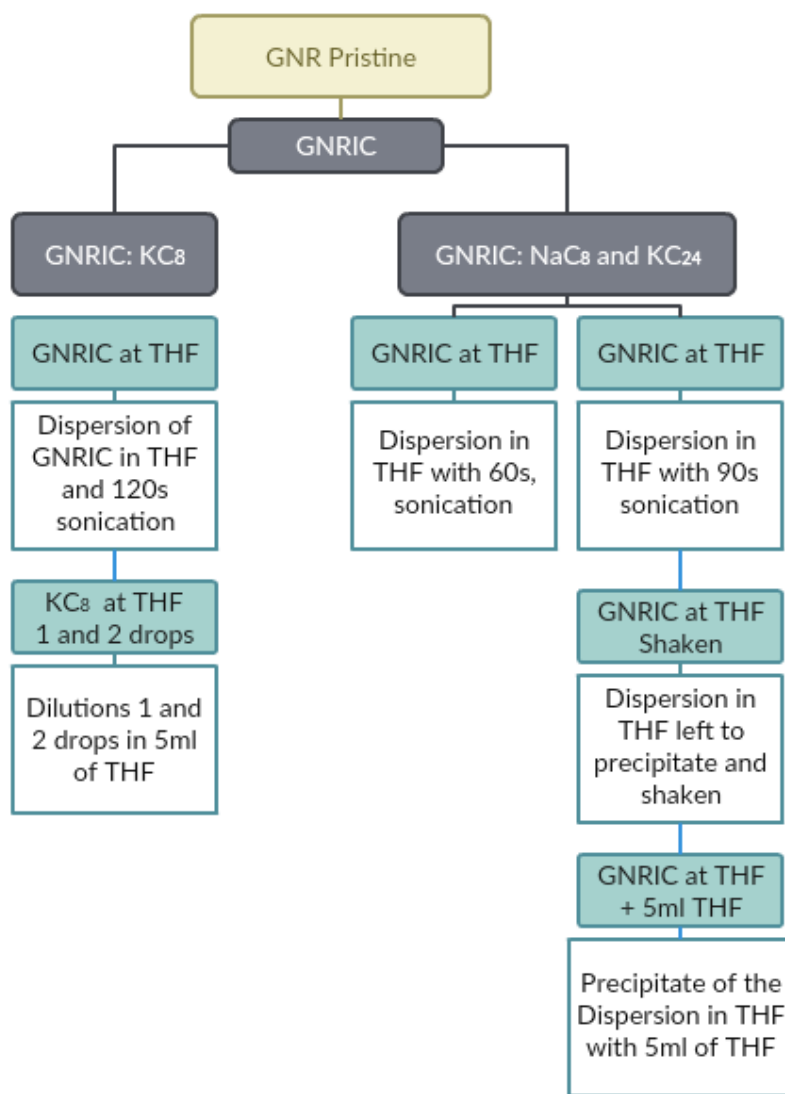
Figure 4.2: Diagram of the experiments performed

Graphene nanoribbons intercalation compounds (GNRICs) of NaC_8, KC_8 and KC_{24} were formed. The stoichiometry of our intercalated compounds were confirmed by Raman spectroscopy based on standard methods.[1,9] GIC and THF were added to a glass vial in a proportion of 0.1 mg per ml. THF solution was previously dried reaching 3.3ppm of H_2O, while sealed and

stored in the glovebox. These solutions were sonicated during 90 seconds with two pulses per second of an ultrasonic tip at 0.465 J [Fig. 4.1]. The solution of KC_8 GNRIC was sonicated 5 minutes with the same tip.

The solutions were left to precipitate for 6 days. We separated the supernatant from the precipitate. The precipitate from each sample was placed into a new glass vial with 5 ml of THF and shaked gently to float the deposited graphene nanoribbons. Figure 4.2 show all the steps of the experiment. The floated GNRs were fished submerging a SiO_2/Si wafer in each solution. The wafers had a 300 nm layer of SiO_2 and were pre-cleaned with acetone and isopropanol using a spin coater. The samples were finally placed in a heating plate a few seconds, in order to evaporate the THF. These steps were repeated for each GNRICs.

The samples obtained were characterized using atomic force microscopy (AFM), scanning electron microscopy (SEM), Raman spectroscopy and Optical Microscopy at the Joint Institute of Advanced Materials and Processes of the University Erlangen-Nuremberg in Germany. Raman spectroscopy characterization was performed using a Horiba LabRAM Aramis and HR evolution spectrometers with a 532 nm laser in all the cases. AFM was carried out in tapping and non-contact modes using a Veeco Dimension 3100 AFM equipment. GNRs were placed on a carbon tape for SEM characterization and analyzed with 5 kV at an Helios NanoLab DualBeam scanning electron microscope.

Chapter 5

Results & Discussion

5.1   Pristine GNRs, KC$_8$ GNRIC and THF dispersion
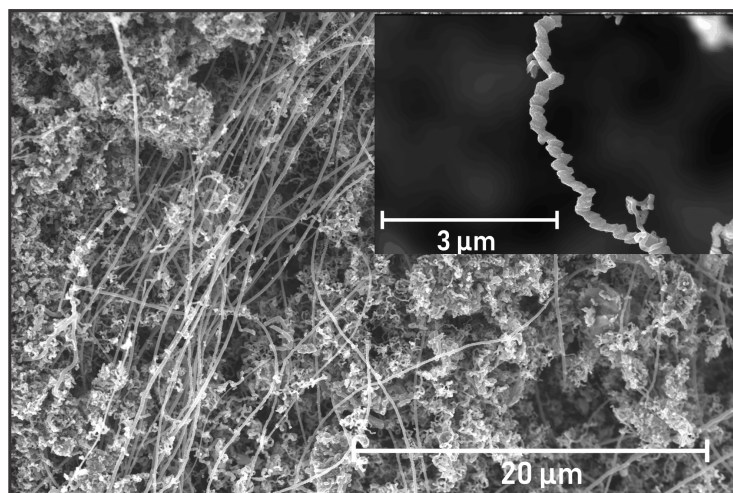
Figure 5.1: SEM micrograph of GNRs pristine sample. At the right corner, magnified SEM micrograph of a GNR pristine is shown

The SEM micrograph of pristine GNRs obtained by CVD are shown in Figure 5.1. We can observe the existence of fiber bundles and other possibly amorphous carbon species in the initial black powder. The fiber morphology is ribbon-like with widths that literature place between 20

nm to 300 nm.[6] The close up image of the ribbon (Figure 5.1 top right) show rippled and flat areas over a GNR. The focus over the GNR in the micrograph make it look individualized, however, it was captured at the edges of the sample and is still part of a GNRs bundle. The estimated thickness obtained by imageJ software over the close up image range from 35 nm to 100 nm. Raman sprectroscopy was used to confirm that this structures are GNRs. The spectrum from this pristine sample is shown in Figure 5.2 bellow.
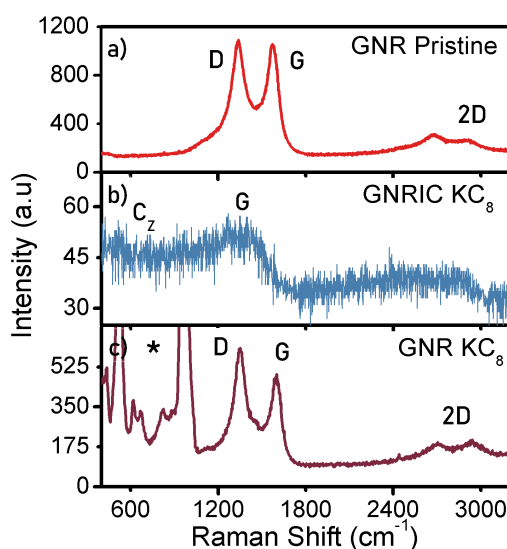
Figure 5.2: Raman spectrum of (a) GNRs pristine, (b) GNR intercalation compound and (c) GNR obtained by KC$_8$ GNRIC dispersion on THF measured with a 532 nm laser.

The Raman spectrum of GNR pristine let us see a D and G-band located at 1338 and 1574 cm^{-1} respectively. There exists a highest intensity on the D-band, caused by the edge and ripple proportion of the GNR[6]. The D/G ratio in this spectrum was found to be 1.25. A possible 2D-band is shown at 2674 cm^{-1}, not completely defined as expected, but recognizable as a peak. D and G position, D/G ratio,and the 2D line presence confirm the existence of GNR structures in the sample.[6]

KC$_8$ GNRIC was the first intercalation compound prepared from the aforementioned pristine GNRs and dispersed in THF. The sample was sonicated during 120 seconds with two pulses per

second with an ultrasonic tip at 0.465 J. This prolonged sonication, could be the most important difference between this sample with respect to the samples prepared after. KC_8 GIC was sealed on a glass tube, in order to avoid a deintercalation caused by the exposure to air during the Raman characterization.[9] The GNRIC KC_8 Raman spectrum [Fig. 5.2 (b)] showed a characteristic broad Fano-line-shape due to the coupling and the interference with the conduction electrons[9] indicating intercalation.[39] Also, a possible C_Z mode is distinguishable at 560 cm^{-1} due to the inter-planar lattice vibrations which indicate a high level of intercalation was achieved.[40] At the bottom [Fig. 5.2 (c)] the dispersed sample raman spectrum, GNR KC_8, show the aforementioned features corresponding to GNRs. The D line is larger with respect with the pristine measurement, then the material is less graphitic (D/G ratio 1.25) than in the pristine case and shows the presence of a peak at 1465 cm^{-1} corresponding to sp^3 carbons due to functionalization strain, possibly -OH groups. There exist a change in lattice distances which provoke five new frequencies appearing between the D and G band[41]. Those vibrations are low, then not so easy to resolve. The most prominent and well located (1465 cm^{-1}) is visible on the analyzed spectrum. This Raman spectrum demonstrated the existence GNRs in the sample. A raman spectrum for comparison of GNRs and GNRIC KC_8 from reference [36] and [22] is shown in figure 5.3
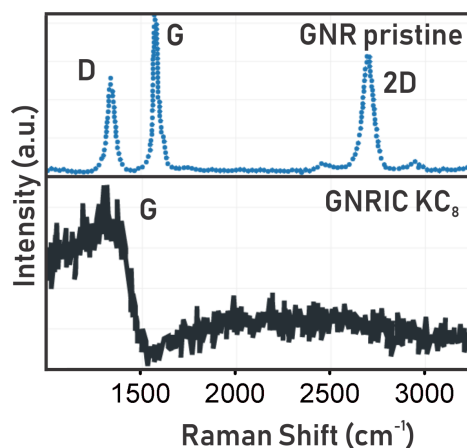
Figure 5.3: Raman spectrum of (a) Graphene nanoribbons pristine and (b) Graphene nanoribbons intercalation compound. Adapted from reference [36][22]
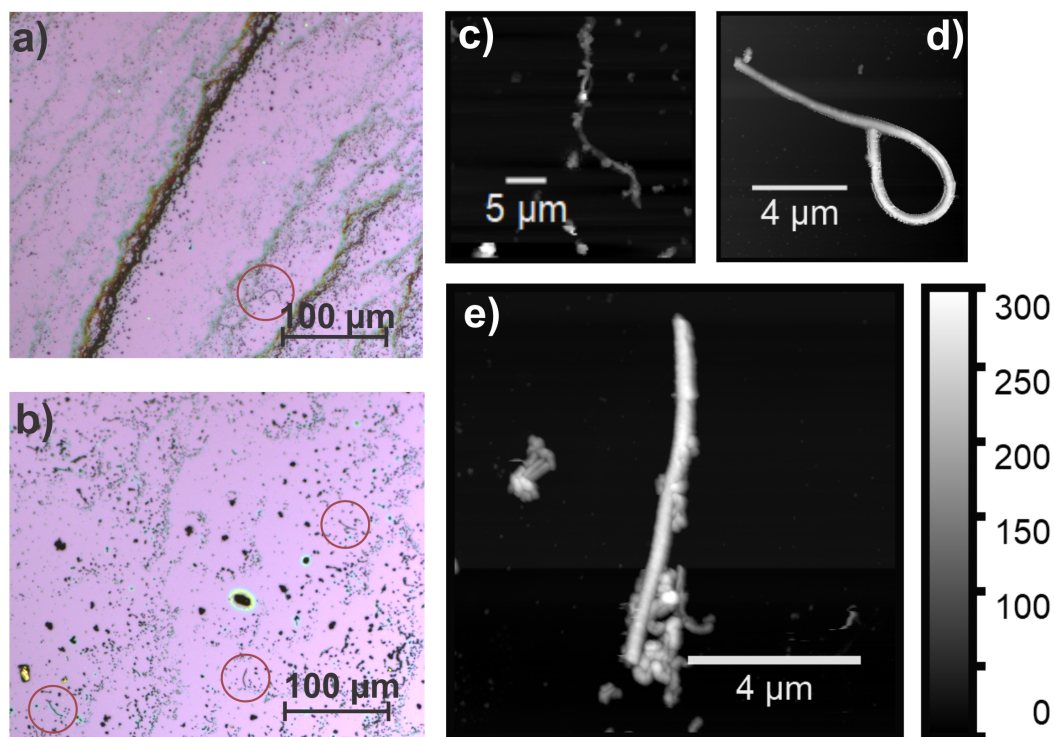
Figure 5.4: Optical Microscope image of KC$_8$ dispersion in THF (a) Supernatant and (b) precipitate. (c)(d)(e) AFM images of GNRs obtained from KC$_8$ supernatant

The optical microscope image shown in figure 5.3 shows the existence of a few ribbons on the samples (a) and (b) (inside the red circles) but a low abundance in KC$_8$ dispersion. The ribbons on the sample [Fig. 5.3 (a) and (b)] x20 magnification showed to be long (from 8 to 23 microns) but few. The thicknes of the GNRs was from 300 nm to 700 nm. The great majority of the SiO_2/Si wafer contained amorphous carbon forms what makes it difficult to observe the GNRs in the sample. The AFM images are shown in figure 5.3 (c), (d) and (e) show the typical cases of GNRs obtained. Some of the GNRs had a good shape and length but were few in the whole sample, an anomaly as the ribbon shown in Figure 5.3 (d). Some others were partially or completely destroyed, possibly by the addition of excessive energy in the sonication [Fig 5.3 (c)]. Other had a uniform edges and long length but had a lot of carbon waste attached to it [Fig 5.3 (e).

Looking at KC$_8$ AFM image [Fig. 5.3 (c, d and e)] was noticeable that the GNRs were unclean

and chopped. Diluted samples (dilution of one and two drops of the GNRIC dispersion on 5ml of THF) of the KC_8 dispersion were prepared and measured, obtaining equal results. Most of the GNRs were destroyed easily while performing Raman measurements. They were fragile and finally discarded.

5.2 SEM, AFM Optical Microscopy Analysis of NaC_8 and KC_{24}

Knowing that the intercalation process was successful on KC_8 and what kind of result was expected, new GNRIC of different stoichiometry were prepared and dispersed, NaC_8 and KC_{24}. The first experiment showed a low amount of GNRs and the reason was not clear. It was theorized that stoichiometry and the size of the ion was the problem. Experiments were performed with a lower amount of alkali metal ion (KC_8) and with a smaller alkali metal ion (NaC_8). The synthesis of those samples was already explained in the methodology section. The samples were measured in three different stages. The dispersions were left to precipitate and shaken. Then, separated into a supernatant and a precipitate to add 5ml of THF on the precipitate flask separated before. The resulting measurements from these samples are shown bellow.
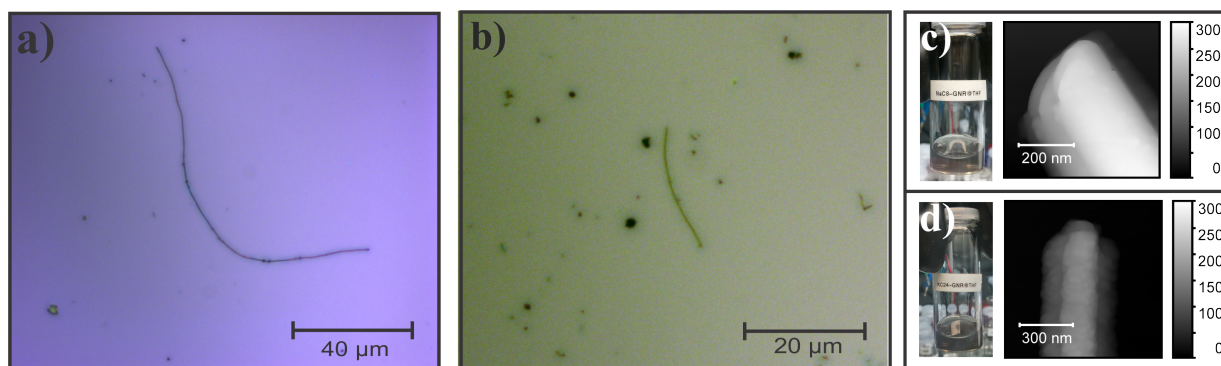
Figure 5.5: (a) Optical microscope image of a GNR at 100x magnification obtained by dispersion of NaC_8 GNRIC and (c) its AFM image. (b) Optical microscope image of a GNR at 100x [Close-up] magnification obtained by dispersion of KC_{24} GNRIC and it (d) AFM image.

Figure 5.4 (a and b) shows the optical results from one of two stages of the experiment. In the first stage, the GNRIC with sodium and potassium [Fig. 5.4 (a,c) and (b,d) respectively] were dispersed and sonicated. The AFM analysis reveals a total thickness of around 250 nm with thinnest layers of 20 nm [Fig. 5.4 (c)] in the Sodium GNRIC dispersion. Also a width of around 600 nm which in general standards is appropriate for a GNR, but creates the need for a driving character analysis in the material.[42] The optical microscope image [Fig. 5.4 (a)] show this sample to be very long, approximately 120 μm, which places it as longer than the synthesized until now as GNRs length is normally in the order of 1 μm.[29,43] In the case of GNR from intercalation with potassium [Fig. 5.4 (b)], the specimens showed a length of 20 μm. Those are still over the standard length.[29,43] At first sight, is found that GNRs in (a) and (b) of figure 5.4 are individualized and do not have carbon byproducts over them. Even the SiO_2/Si wafer is almost clean of waste, especially in the sample dispersed from sodium GNRIC [Fig. 5.4 (a)]. The opacity of the GNR in Figure 5.4 (b) gave us hints about a lower thickness with respect to Figure 5.4 (b), analyzed following through the AFM image of this specific GNR. The Figure 5.4 (a) also shows areas of less intensity on the color of the ribbon, it is caused not by its thickness but by the contact with the wafer, which in this case is not complete and cause these areas to be out of focus and look blurry. The AFM image [Fig 5.4 (d)] shows a decrease in the width of the GNR, and the layer look more homogeneus in shape compared with the GNRs analyzed from dispersion of GNRIC NaC$_8$. This GNR width is around 400 nm and posses a thickness peak at 154 nm. Its thinnest visible layer posses 30 nm, which is consistent with the pristine GNRs thickness analyzed before.
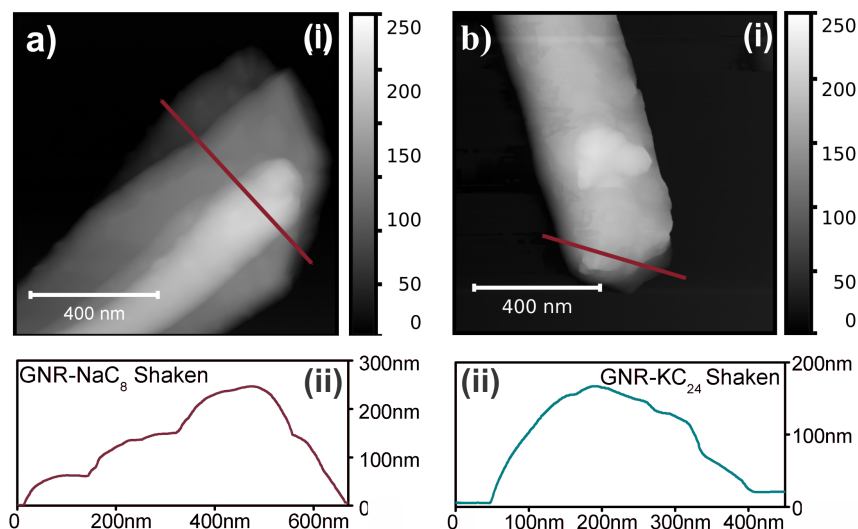
Figure 5.6: [(a) (i) AFM image of GNR-NaC$_8$ shaken.(ii) Profile plot of GNR-NaC$_8$ shaken. (b) (i) AFM image of GNR-KC$_{24}$ shaken.(ii) Profile plot of GNR-KC$_{24}$ shaken.

During a second process performed, the sample was left to precipitate for several days and then shaken to detect a possible re-dispersion process of GNRIC. The AFM profile of KC$_{24}$ shaken sample [Fig. 5.5 (b)(ii)] show a rounded shape profile which hamper the possibility of loop formation, making recommendable to perform a Raman analysis to detect it in case of existing. Figure 5.5 (b)(i) show uniformity on the width of its layers, also some waste above it. Figure 5.5(a)(i) show wider layers at the bottom of the GNR and an accumulation of narrow layers at the center. These characteristics raise suspicions of an agglomeration of GNR layers after the exfoliation.

AFM images [Fig. 5.5 (a)(ii) and (b)(ii)] showed widths from 400-600 nm and a maximum thickness of 240 nm and 180 nm approximately for NaC$_8$ and KC$_{24}$ shaken samples respectively. This thickness analysis show us a tendency of KC$_{24}$ dispersion to have thinner GNRs, hence less layers than NaC$_8$ dispersion.
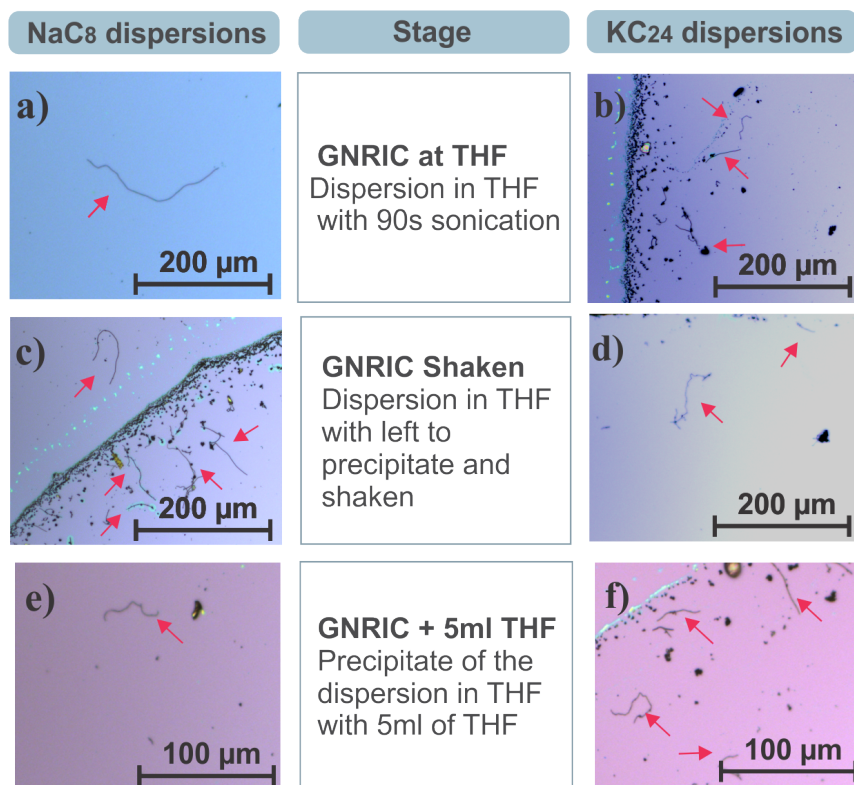
Figure 5.7: Optical microscope image of a) NaC$_8$ and b) KC$_{24}$ GNRIC @ THF. c) NaC$_8$ and d) KC$_{24}$ GNRIC left to precipitate and shaken. e) NaC$_8$ and f) KC$_{24}$ GNRIC refilled with THF. In the last process the GNRs were left to precipitate and separated in precipitate and supernatant. The precipitate flask was filled with 5ml of THF

A third procedure on the sample discussed before consisted of separating the sample into precipitate and supernatant and refilling with 5ml of THF the precipitate flask. Then, agitating the sample in order to make the GNRs contained in the precipitate float and look for a second dispersion process. The optical microscope images of the three most important stages explained are showed to gave us hints about the behavior of the material [Fig. 5.6]. The third procedure show us clean and long GNRs for both dispersion [Fig. 5.6 (e and f)]. The length is consistent with the other stages explained before while the abundance has decreased in NaC$_8$ dispersion [Fig. 5.6 (e)] with respect to the previous procedure shown in figure 5.6 (c). In general, exists a tendency of NaC$_8$ to produce larger GNRs while KC$_8$ to produce a larger amount of them. The

three steps showed GNRs located at the supernatant of the sample are the largest amount in the case of sodium while the opposite on the case of potassium. The third process exposes this fact as the precipitate was separated and refilled. Then, it indicates that in KC_{24} GNRIC precipitate contained the largest amount of GNRs [Fig. 5.6]. All the stages of NaC_8 and KC_{24} dispersion revealed a great amount of individualized GNRs, many with lengths greater than $20\,\mu$m. However, there is still a need for further characterization to determine the electronic character of the GNRs.

5.3   Raman Spectroscopy Analysis of NaC_8 and KC_{24}
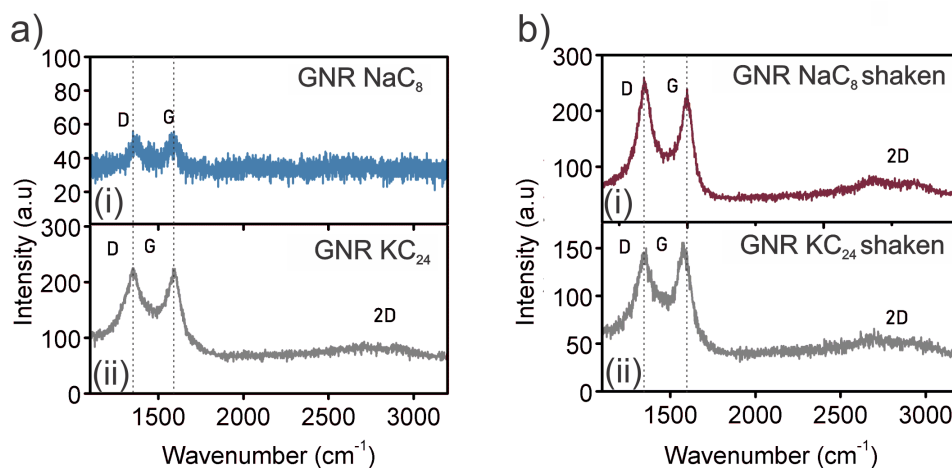
Figure 5.8: (a) Raman spectrum of GNR NaC_8 and GNR KC_{24} dispersed in THF measured with a 532 nm laser. (b) Raman spectrum of GNR NaC_8 and GNR KC_{24} dispersed in THF after shaken process measured with a 532 nm laser.

Figure 5.7 show four Raman spectrum with GNR features (discused in the section 5.1). Figure 5.7 (a)(i) show a 1.01 D/G ratio and a very low number of counts possibly caused by the focus over the sample, which was not good as the GNR was not fully seated on the wafer in many cases. Been the fist sample of this kind to be measured, the tendency on how many counts per sample could be obtained was not clear, and the low counting was misinterpreted as low amounts of layers. The spectrum also show a peak at around 1450 cm^{-1} which correspond to lattice embedded sp^3

carbon atoms which indicate functionalization[41]. This feature was already explained in section 5.1. Figure 5.7 (a)(ii) show a greater number of counts than the spectrum of NaC$_8$ dispersion. It also shows a shoulder on the G line, possibly caused by the addition of functional groups causing strain and a slight spliting of the line into two frequencies. The spectrums in figure 5.7 (b) exhibit a great difference in the D/G ratio between them. NaC$_8$ show a larger D/G ratio than KC$_{24}$ shaken dispersión (0.98 and 0.94). The intensity the D line indicate the proportion of defects in the sample, which is normally high in GNRs as the edges appear in the spectrum as defects.[1] The diminution of the ratio, could be caused by the addition of functional groups to the edges of the KC$_{24}$ GNRs.

Sample	ID/IG Ratio
NaC$_8$	1.01
KC$_{24}$	1
NaC$_8$ Shaken	0.98
KC$_{24}$ Shaken	0.94

Table 5.1: Intensity ratio of D and G line of NaC$_8$ and KC$_{24}$ spectrum immediately measured and after shaken.

The split in the 2D line in NaC$_8$ dispersion spectrum [Fig. 5.7 (b)(i)] is common in GNRs due to the double resonance processes done by the D and G modes.[23] KC$_{24}$ [Fig. 5.7 (b)(ii)] do not show it clearly because of the low intensity of counts caused by the thickness of the material or/and the low laser power used, necessary to preserve the sample. This double resonant feature could be present as the split even in three modes at high frequencies depending on the stacking and number of layers of the material[23].

The crystallinity seem to be higher in KC$_{24}$ shaken sample [Fig. 5.7 (b)(ii)]. There exists a red shift of the G line (1578 cm^{-1}) of around 15 wave numbers with respect to the previous process spectrum and its analog prepared with sodium. The addition of impurities on the material, n-type doping, after the re-dispersion is a possible cause of this shift. The laser power was at 10/100 of its capacity in each of the sample measurement. Then, is improbable that the increment of the temperature done by the laser energy caused that specific shift. GNR KC$_{24}$ shaken Raman spectrum shows the reduction of the D line which suggest that defects of the edges of the sample were eliminated. This information and 5.5 (b) (ii) AFM image can lead to thinking on the

formation of a loop structures in the material after the re-dispersion[44], however, the 2D modes did not show a significant increment with respect to the no re-dispersed Raman spectrum [Fig. 5.7 (a) Bottom], dismissing this possibility.[44]

Chapter 6

Conclusion and Outlook

In this work, I have studied the dispersion of alkali metal intercalated graphene nanoribbons. As first approach, I produced KC_8 intercalation compound and dispersed it in dried THF solvent. The optical microscope and Raman spectrometer showed KC_8 samples contain almost no GNR. KC_{24} and NaC_8 intercalation compounds were prepared and sonicated with two pulses per second of an ultrasonic tip at 0.465 J during 90 seconds. Optical microscopy showed very large and individualized specimens. Those samples were left to precipitate and shook before 6 days. The next experiment consisted in separating precipitate and supernatant part, then the precipitate was refill with 5 ml of THF. The three steps showed GNRs located at the supernatant of the sample are the largest amount in the case of sodium while the opposite on the case of potassium. The following process exposed this fact as the precipitate was separated and refilled and the assumption presented before was still consistent. Then, it indicates that in KC_{24} GNRIC precipitate contained the largest amount of GNRs. The difference in large and width of the GNRs from KC_{24} and NaC_8 dispersions could be caused by the alkali metal ions used in each case. The ionic radii of Na, shorter than K ionic radii, would cause a less ruptures on the GNRs structure. During the exfoliation, its size could allow them to go out from between the layers in an easier way than the potassium ions. The lower probability of rupture could lead to larger GNRs, but with a larger amount of layers, and the opposite case in potasium intercalation/exfoliation process. The AFM image of the samples showed GNRs with widths in the range of aproximately 400 nm to 600 nm, thick from 150 nm to 250 nm and large of hundred of micrometers.

NaC_8 intercalation showed a larger defect ratio than KC_{24}, possibly due to a higher rate of in-

clusion of functional groups at the edges. Pristine graphene nanoribbons were thin (around 30 nm) and long, but entangled. The AFM profile reveled layers in the structure of around 20 to 30 nm. The larger thickness of the GNRs could be caused by the agglomeration of the dispersed graphene nanoribbons layers after the exfoliation. All the stages revealed very large individual-ized GNRs.The method described in this work show a simple and low cost procedure to obtain GNRs for scalable production. There is still a need for further characterization to determine the electronic character of the GNRs obtained, however, their ribbon-like shape, and great length place them as very promising to be integrated into nanodevices.

Bibliography

[1] Nakada, K.; Fujita, M.; Dresselhaus, G.; Dresselhaus, M. S. Edge state in graphene ribbons: Nanometer size effect and edge shape dependence. *Physical Review B* **1996**, *54*, 17954–17961.

[2] Zhang, T.; Wu, S.; Yang, R.; Zhang, G. Graphene: Nanostructure engineering and applications. *Frontiers of Physics* **2017**, *12*.

[3] Celis, A.; Nair, M. N.; Taleb-Ibrahimi, A.; Conrad, E. H.; Berger, C.; de Heer, W. A.; Tejeda, A. Graphene nanoribbons: fabrication, properties and devices. *Journal of Physics D: Applied Physics* **2016**, *49*, 143001.

[4] Hawkins, P.; Begliarbekov, M.; Zivkovic, M.; Strauf, S.; Search, C. P. Quantum Transport in Graphene Nanoribbons with Realistic Edges. *The Journal of Physical Chemistry C* **2012**, *116*, 18382–18387.

[5] Mathur, R. B.; Singh, B. P.; Pande, S. *Carbon Nanomaterials*; Taylor & Francis Inc, **2017**.

[6] Campos-Delgado, J. *et al.* Bulk Production of a New Form of sp2Carbon: Crystalline Graphene Nanoribbons. *Nano Letters* **2008**, *8*, 2773–2778.

[7] Xu, Y.; Cao, H.; Xue, Y.; Li, B.; Cai, W. Liquid-Phase Exfoliation of Graphene: An Overview on Exfoliation Media, Techniques, and Challenges. *Nanomaterials* **2018**, *8*, 942.

[8] Pénicaud, A.; Poulin, P.; Derré, A.; Anglaret, E.; Petit, P. Spontaneous Dissolution of a Single-Wall Carbon Nanotube Salt. *Journal of the American Chemical Society* **2005**, *127*, 8–9.

[9] Chacón-Torres, J. C.; Wirtz, L.; Pichler, T. Raman spectroscopy of graphite intercalation compounds: Charge transfer, strain, and electron-phonon coupling in graphene layers. *physica status solidi (b)* **2014**, *251*, 2337–2355.

[10] Jia, X.; Campos-Delgado, J.; Terrones, M.; Meunier, V.; Dresselhaus, M. S. Graphene edges: a review of their fabrication and characterization. *Nanoscale* **2011**, *3*, 86–95.

[11] Terrones, M.; Botello-Méndez, A. R.; Campos-Delgado, J.; López-Urías, F.; Vega-Cantú, Y. I.; Rodríguez-Macías, F. J.; Elías, A. L.; Muñoz-Sandoval, E.; Cano-Márquez, A. G.; Charlier, J.-C. Graphene and graphite nanoribbons: Morphology, properties, synthesis, defects and applications. *Nano Today* **2010**, *5*, 351–372.

[12] Dutta, S.; Pati, S. K. Novel properties of graphene nanoribbons: a review. *Journal of Materials Chemistry* **2010**, *20*, 8207.

[13] Dennison, J.; Holtz, M. Raman spectroscopy of carbon materials. *Spectroscopy (Santa Monica)* **1996**, *11*, 38–46.

[14] Deng, Y.; Cranford, S. W. Thermal conductivity of 1D carbyne chains. *Computational Materials Science* **2017**, *129*, 226–230.

[15] Liu, M.; Artyukhov, V. I.; Lee, H.; Xu, F.; Yakobson, B. I. Carbyne from First Principles: Chain of C Atoms, a Nanorod or a Nanorope. *ACS Nano* **2013**, *7*, 10075–10082.

[16] Kern, F.; Bernstein, A.; Killinger, A. *Advances in Ceramic Biomaterials*; Elsevier, **2017**, pp 331–353.

[17] Milne, W.; Robertson, J. *Encyclopedia of Materials: Science and Technology*; Elsevier, **2001**, pp 900–902.

[18] Ehrenfreund, P.; Foing, B. H. Fullerenes and Cosmic Carbon. *Science* **2010**, *329*, 1159–1160.

[19] ichi Fujita, J.; Hiyama, T.; Hirukawa, A.; Kondo, T.; Nakamura, J.; ichi Ito, S.; Araki, R.; Ito, Y.; Takeguchi, M.; Pai, W. W. Near room temperature chemical vapor deposition of graphene with diluted methane and molten gallium catalyst. *Scientific Reports* **2017**, *7*.

[20] Saito, R.; Hofmann, M.; Dresselhaus, G.; Jorio, A.; Dresselhaus, M. S. Raman spectroscopy of graphene and carbon nanotubes. *Advances in Physics* **2011**, *60*, 413–550.

[21] Sevinçli, H.; Topsakal, M.; Ciraci, S. *Low Dimensional Semiconductor Structures*; Springer Berlin Heidelberg, **2012**, pp 69–92.

[22] Kan, E.; Li, Z.; Yang, J. *Physics and Applications of Graphene - Theory*; InTech, **2011**.

[23] Jorio, A.; Saito, R.; Dresselhaus, G.; Dresselhaus, M. S. *Raman Spectroscopy in Graphene Related Systems*; Wiley-VCH Verlag GmbH & Co. KGaA, **2011**.

[24] Han, M. Y.; Özyilmaz, B.; Zhang, Y.; Kim, P. Energy Band-Gap Engineering of Graphene Nanoribbons. *Physical Review Letters* **2007**, *98*.

[25] Kimouche, A.; Ervasti, M. M.; Drost, R.; Halonen, S.; Harju, A.; Joensuu, P. M.; Sainio, J.; Liljeroth, P. Ultra-narrow metallic armchair graphene nanoribbons. *Nature Communications* **2015**, *6*.

[26] Wakabayashi, K. *Graphene Nanoelectronics*; Springer Berlin Heidelberg, **2011**, pp 277–299.

[27] Wang, S.; Wang, C.; Ji, X. Towards understanding the salt-intercalation exfoliation of graphite into graphene. *RSC Advances* **2017**, *7*, 52252–52260.

[28] Xu, W.; Lee, T.-W. Recent progress in fabrication techniques of graphene nanoribbons. *Materials Horizons* **2016**, *3*, 186–207.

[29] Cortizo-Lacalle, D.; Mora-Fuentes, J. P.; Strutyński, K.; Saeki, A.; Melle-Franco, M.; Mateo-Alonso, A. Monodisperse N-Doped Graphene Nanoribbons Reaching 7.7 Nanometers in Length. *Angewandte Chemie International Edition* **2017**, *57*, 703–708.

[30] Clayden, J. Deconstructing THF. *Nature Chemistry* **2010**, *2*, 523–524.

[31] Binnig, G.; Quate, C. F.; Gerber, C. Atomic Force Microscope. *Physical Review Letters* **1986**, *56*, 930–933.

[32] Haugstad, G. *Atomic Force Microscopy*; John Wiley & Sons, Inc., **2012**.

[33] de Pablo, P. J. *Single Molecule Analysis*; Humana Press, **2011**, pp 197–212.

[34] Zhou, W.; Apkarian, R.; Wang, Z. L.; Joy, D. *Scanning Microscopy for Nanotechnology*; Springer New York, **2006**, pp 1–40.

[35] Beams, R.; Cançado, L. G.; Novotny, L. Raman characterization of defects and dopants in graphene. *Journal of Physics: Condensed Matter* **2015**, *27*, 083002.

[36] Wang, W.; McGregor, H.; Short, M.; Zeng, H. Clinical utility of Raman spectroscopy: current applications and ongoing developments. *Advanced Health Care Technologies* **2016**, 13.

[37] Gracia-Espino, E.; López-Urías, F.; Kim, Y.; Hayashi, T.; Muramatsu, H.; Endo, M.; Terrones, H.; Terrones, M.; Dresselhaus, M. S. *Handbook of Advanced Ceramics*; Elsevier, **2013**, pp 61–87.

[38] Smith, E.; Dent, G. *Modern Raman Spectroscopy: A Practical Approach*; **2005**.

[39] Vecera, P.; Holzwarth, J.; Edelthalhammer, K. F.; Mundloch, U.; Peterlik, H.; Hauke, F.; Hirsch, A. Solvent-driven electron trapping and mass transport in reduced graphites to access perfect graphene. *Nature Communications* **2016**, *7*.

[40] Chacón-Torres, J. C.; Ganin, A. Y.; Rosseinsky, M. J.; Pichler, T. Raman response of stage-1 graphite intercalation compounds revisited. *Physical Review B* **2012**, *86*.

[41] Vecera, P.; Chacón-Torres, J. C.; Pichler, T.; Reich, S.; Soni, H. R.; Gröling, A.; Edelthalhammer, K.; Peterlik, H.; Hauke, F.; Hirsch, A. Precise determination of graphene functionalization by in situ Raman spectroscopy. *Nature Communications* **2017**, *8*.

[42] Son, Y.-W.; Cohen, M. L.; Louie, S. G. Energy Gaps in Graphene Nanoribbons. *Physical Review Letters* **2006**, *97*.

[43] Giovannantonio, M. D.; Deniz, O.; Urgel, J. I.; Widmer, R.; Dienel, T.; Stolz, S.; Sánchez-Sánchez, C.; Muntwiler, M.; Dumslaff, T.; Berger, R.; Narita, A.; Feng, X.; MÃijllen, K.; Ruffieux, P.; Fasel, R. On-Surface Growth Dynamics of Graphene Nanoribbons: The Role of Halogen Functionalization. *ACS Nano* **2017**, *12*, 74–81.

[44] Jia, X.; Campos-Delgado, J.; Gracia-Espino, E. E.; Hofmann, M.; Muramatsu, H.; Kim, Y. A.; Hayashi, T.; Endo, M.; Kong, J.; Terrones, M.; Dresselhaus, M. S. Loop formation in graphitic nanoribbon edges using furnace heating or Joule heating. *Journal of Vacuum Science & Technology B: Microelectronics and Nanometer Structures* **2009**, *27*, 1996.